Published in final edited form as:
J Dent Res. 2006 April ; 85(4): 359–363.

Enamel Demineralization in Primary and Permanent Teeth

L.J. Wang[1], **R. Tang**[1], **T. Bonstein**[2], **P. Bush**[2], and **G.H. Nancollas**[1,*]

1 *Department of Chemistry, 750 Natural Sciences Complex, University at Buffalo, The State University of New York, Buffalo, NY 14260, USA*

2 *School of Dental Medicine, 750 Natural Sciences Complex, University at Buffalo, The State University of New York, Buffalo, NY 14260, USA*

Abstract

Although enamel demineralization is important for our understanding of caries formation, no consensus has been reached regarding the possible differences in susceptibility of primary and permanent enamel. We used the constant composition (CC) technique to investigate the acid-induced demineralization of these tissues at a relative undersaturation with respect to hydroxyapatite (HAP) of 0.902, pH = 4.5, and ionic strength = 0.15 mol L^{-1}. The demineralization rates showed significant differences, primary enamel having the greater susceptibility to dissolution during an initial linear stage: $1.5 \pm 0.5 \times 10^{-10}$ mol mm^{-2} min^{-1} compared with $2.6 \pm 0.5 \times 10^{-11}$ mol mm^{-2} min^{-1} for permanent enamel. During the reactions, we observed nanosized crystallites which attached to the enamel surfaces or escaped into the bulk solution. These nanosized crystallites were kinetically protected against further dissolution, even though the solutions remained undersaturated. It is hypothesized that they may contribute to the remarkable mechanical and dynamic characteristics of enamel.

Keywords

demineralization; constant composition; primary enamel; permanent enamel; nanoparticle

INTRODUCTION

The demineralization of dental enamel is of particular clinical relevance, and several studies have investigated possible differences between the susceptibility of primary (deciduous) and permanent enamel to erosion. Results have been contradictory, showing either a higher susceptibility of deciduous enamel to erosion (50% greater mineral loss, and 30% lesion depth) (Amaechi *et al.*, 1999; Hunter *et al.*, 2000), or no statistically significant differences (Maupome *et al.*, 1999; Issa *et al.*, 2003). Primary enamel, however, exhibits morphological differences: It is less-mineralized than permanent enamel, and the diffusion coefficient is greater in primary than in permanent enamel (Linden *et al.*, 1986). Overall mineral density was lower in the outermost layers, but showed no significant differences close to the enamelo-dentinal junction (Wilson and Beynon, 1989). *In vitro* nanoindentation studies, combined with atomic force microscopy in the early demineralization stages, suggested that the primary enamel was not more susceptible to erosion (Lippert *et al.*, 2004), even though it was reported to be statistically significantly softer and less elastic (Lussi *et al.*, 2000).

In this work, the susceptibility to acid-induced demineralization in vitro and differences in ultrastructure and dissolution kinetics of primary and permanent tooth enamel were studied by

corresponding author, E-mail: ghn@buffalo.edu.

a constant composition (CC) technique. The relative undersaturation with respect to HAP was 0.902, with pH = 4.5 and ionic strength = 0.15 mol L^{-1}.

MATERIALS & METHODS

Twenty freshly extracted caries- and filling-free human primary and permanent molars, stored for less than 2 wks in 0.5% Chloramine-T, were used. We cut each tooth horizontally at the cemento-enamel junction to remove the root portion. We cut the crown vertically (parallel to the tooth axis) from the buccal and lingual sides to produce 2 enamel discs about 2 mm thick from each tooth (40 discs in all). All cuts were made with the use of a slow-speed diamond saw (Buehler Isomet 1000 precision saw, Lake Bluff, IL, USA) with water irrigation. Samples were cleaned by ultrasonication in distilled water for 5 min before and after being polished, and were serially polished with progressively finer silicon carbide papers (P800, P1000, P1200, P2400 and P4000) (Struers, Copenhagen, Denmark). The use of human tissue specimens followed a protocol that was approved by our IRB/ethical committee, and informed patient consent was obtained.

In the constant composition (CC) method (Tomson and Nancollas, 1978), multiple titrant solutions containing HCl and NaCl were added simultaneously to the reaction solutions during the reactions. Titrants were prepared according to eqns. (1) and (2), taking into account dilution effects.

$$T_{NaCl} = W_{NaCl} + 6C_{eff} \tag{1}$$

$$T_{HCl} = 14C_{eff} \tag{2}$$

In eqns. (1) and (2), W and T are the total concentrations in the reaction solutions and titrants, respectively; and C_{eff} is the effective titrant concentration with respect to HAP (C_{eff} = 1.00 × $10^{-}4$ mol L^{-1}).

CC curves, recorded as plots of added titrant volume, V, against time, t, were used to calculate the dissolution rates, R, from eqn. 3

$$R = (C_{eff}/A_T) \cdot (dV/dt) \tag{3}$$

The dissolution rate is expressed as equivalent moles of HAP dissolved *per* mm^2 of surface *per* min. A_T is the geometric surface area of enamel exposed to the reaction solutions.

The dissolution experiments, initiated by the introduction of known amounts of enamel sample, were conducted in magnetically stirred (450 rpm) double-walled Pyrex vessels thermostated at 37.0 ± 0.1°C. Undersaturated solutions, prepared by the mixing of calcium chloride and potassium dihydrogen phosphate with sodium chloride to maintain the ionic strength at 0.15 mol L^{-1}, were adjusted to pH = 4.50 by the dropwise addition of HCl (0.05 mol L^{-1}). The relative undersaturation with respect to HAP, σ, is defined by eqn.4:

$$\sigma = 1 - S = 1 - \left[\frac{IAP}{K_{sp}}\right]^{1/v} \tag{4}$$

where S is the undersaturation ratio, v is the number of ions in a formula unit of the salt, and IAP and K_{sp} are the ionic activity and solubility products, respectively (Mullin, 2001;Tang *et al.*, 2001).

$$S=\left[\frac{(Ca^{2+})^{10}(PO_4^{3-})^6(OH^-)^2}{K_{sp}}\right]^{1/18} \quad (5)$$

where (Ca^{2+}), (PO_4^{3-}), and (OH^-) are calculated by the PHREEQE speciation program, with the Davies extended form of the Debye-Hückel equation, using mass balance expressions for total calcium and total phosphate with appropriate equilibrium constants by successive approximation for the ionic strength. K_{sp} is the solubility product at 37.0°C (5.52×10^{-118}). A σ value of 0.902 was achieved by the use of total molar concentrations: calcium, 1.00×10^{-3} mol L^{-1}; phosphate, 6.00×10^{-4} mol L^{-1}; and sodium chloride, 0.146 mol L^{-1}.

Titrant addition was triggered by a potentiometer (Orion 720A, Beverly, MA, USA) incorporating glass (Orion No. 91-01, USA) and reference Ag/AgCl (Orion 900100, USA) electrodes. During the dissolution, the electromotive force was constantly compared with a preset value, and the difference, or error signal, activated motor-driven titrant burets to maintain a constant thermodynamic dissolution driving force. During the reactions, samples were periodically withdrawn and filtered (0.22 μm Millipore filters, Sterlitech, Kent, WA, USA), and the solutions were analyzed for total calcium (atomic absorption) and phosphate (spectrophotometrically as the vanado-molybdate complex); concentrations remained constant to within 1%.

Crystallites for SEM investigation (Hitachi S-4000 FESEM, beam voltage at 20 kV, HITACHI Ltd, Schaumburg, IL, USA) were collected from the bulk solution by filtration (Nucleopore N003 filter membranes), both during and at the end of the dissolution experiments, and were dried at room temperature.

RESULTS

When smear layers had been completely removed, native enamel surfaces were exposed to the reaction solutions. Scanning electron microscopic (SEM) examination of the resulting etched primary and permanent enamel surfaces showed that demineralization, initiated at core(prism or rod)/wall(prism sheath) interfaces, developed anisotropically along the *c*-axes (Fig. 1). During dissolution, crystallites became smaller, and eventually nanosized crystallites were observed to attach to the primary enamel surface (Figs. 2a, 2b), or escaped into the bulk solution (Fig. 2c). After further dissolution, enamel walls of the primary teeth tended to fracture, while permanent enamel walls remained intact (Fig. 3). It has been shown that almost all of the organic components in enamel are located in the walls (Pelton *et al.*, 1991;Veis, 2003), but it is not clear how matrix proteins contribute to the mechanical properties of the enamel.

After long reaction times (1 to 2 wks), nanosized apatite particles collected from the bulk solution by filtration were kinetically protected against further dissolution, even though the solutions remained undersaturated (Fig. 4). From the CC curves, the mean dissolution rates of primary and permanent tooth enamel during the initial linear stage of dissolution were $1.5 \pm 0.5 \times 10^{-10}$ mol mm^{-2} min^{-1} and $2.6 \pm 0.5 \times 10^{-11}$ mol mm^{-2} min^{-1}, respectively (Fig. 4e).

DISCUSSION

In most kinetic studies, the dissolution rate *R* has been empirically expressed by a rate law such as eqn. 6,

$$R=k\sigma^{n}=k(1-S)^{n} \quad (6)$$

where *k* is the rate constant, and *n* is the effective reaction order (n = 1 for diffusion control). Eqn. 6 implies that the dissolution rate should remain constant at sustained undersaturation. It is well-known that the dissolution of calcium phosphate crystals is highly dependent on the degree of saturation, *S*. Previously, it was considered that when $S < 1$, and with a constant value of *S* maintained, all crystals would inexorably dissolve, until the solid phases had disappeared. However, recent CC studies have shown that the rates decrease markedly with time, despite sustained undersaturations (Tang *et al.*, 2004). Microradiography combined with densitometric analysis showed that the surface layer and the interior part of natural caries lesions possessed a high degree of resistance to acid attack, relative to the underlying normal enamel (Aoba and Yagi, 1982). This phenomenon of experimentally observed self-inhibiting dissolution of HAP was also reported previously (Mafe *et al.*, 1992).

For all the enamel samples, the initial loss of mineral with time was nearly linear (Fig. 4e). Our recent results also showed that the rates of mineral loss perpendicular and parallel to the enamel rod *c*-axis were both approximately constant, but different (Wang *et al.*, 2005). This anisotropy supports the suggestion (Anderson *et al.*, 1998;Ando *et al.*, 2001;Dowker *et al.*, 2003) that the rate of demineralization depends on the direction and position of the acid attack within a developing lesion. However, the CC results show that this inhomogeneity does not appear to influence the linearity of the mineral loss with time (Fig. 4e). For *in situ* demineralization, both the lesion depth and the mineral loss varied linearly with demineralization time, but *in vitro* lesion depth increased with a fractional power of time (1/2 or 1/3) (Arends *et al.*, 1992).

Since the composition and structure of enamel tissues are inhomogeneous and change with lesion development, the process of demineralization is expected to be complex, even in an *in vitro* model system. In the light of the different dissolution rates of primary and permanent enamel, the direct assumption is that rate differences arise from differences in structure (Shellis, 1984; Sonju Clasen *et al.*, 1997). Mean lesion depths were associated with prism-junction density and volume fraction of interprismatic enamel, where both were significantly greater in primary enamel than in its permanent counterpart (Shellis, 1984). The accessible pore volume in partially demineralized enamel influences the distribution of subsequent mineral loss. The effects might be mediated by changes in ion transport, induced by local diffusion coefficients with changing porosity (Dowker *et al.*, 2003) and the relative mineral contents (Naujoks *et al.*, 1967). The reported mineral content is 81.3–94.2 wt% for primary enamel (Angker *et al.*, 2004; Cuy *et al.*, 2002), while permanent enamel is close to pure synthetic apatite (around 97%), with the remainder consisting of water and organic matrix (LeGeros, 1991); matrix proteins are essentially removed during mature enamel formation (Veis, 2003). Typically, organic components inhibit crystal dissolution (Weiner and Dove, 2003). However, in this study, primary enamel with higher organic content dissolved considerably faster than permanent enamel. The demineralization of primary and permanent enamel in acidic media showed significant differences, with primary enamel having a greater susceptibility to demineralization (Fig. 4e).

The major event in early enamel crystal dissolution is preferential dissolution along a central defect (Johnson, 1967; Orams *et al.*, 1980). Arends and Jongebloed (1977) indicated that the unusual dissolution behavior of enamel can be related to dislocations. These dislocations, or

linear lattice defects, are present in the crystallite centers, and, as a result of acid attack, are the source of two active dissolution sites in each crystallite (Arends and Jongebloed, 1977; Jongebloed *et al.*, 1975). Simmelink *et al.* (1974) clearly showed acid-treated human enamel crystals with concave ends along the middle line of crystallite c-axes.

Thickness and width measurements of human enamel crystallites in their mature stage are 26.3 ± 2.2 nm and 68. 3 ± 13.4 nm, respectively (Kerebel *et al.*, 1979); however, the length is in the range of 100–1000 nm (Tesch *et al.*, 2001). Therefore, the central defects on the large crystallite faces provide active dissolution sites, and result in rapid fragmentation of the crystals (Simmelink *et al.*, 1974; Jongebloed *et al.*, 1975) into small pieces (Figs. 4a, 4b).

The dislocations or central defects were similar to the active pits in our dissolution model, and the previous observations are consistent with our results and the suggested model. In both cases, the CC dissolution reactions were suppressed when the crystallites approached critical sizes (r^*) in the nanoscale (Wang *et al.*, 2005). Demineralization of sparingly soluble salts, such as apatite, was generally initiated and accompanied by the formation and development of pits on the crystal surfaces, and the dissolution rates were also determined by the pit densities and step-spreading velocities. It has been shown that only pits which are larger than r^* provide the active dissolution sites that contribute to dissolution (Tang *et al.*, 2001). When r is closer to r^*, there is no fast movement of the stepwave, and the macroscopic dissolution rate is markedly reduced, approaching zero, despite the sustained driving force. The estimated value of r^* is about 40–50 nm under these dissolution conditions (Wang *et al.*, 2005). It is significant that the collected residues following enamel dissolution have similar size distributions (Figs. 4a, 4b). These nanosized enamel crystallites will be expected to show a remarkable degree of self-preservation (Tang *et al.*, 2004) in the fluctuating physiological milieu, and, in association with organic components, may contribute to the physical characteristics of dental enamel.

Acknowledgments

This work was supported by National Institutes of Health (NIDCR DE03223).

References

Amaechi BT, Higham SM, Edgar WM. Factors influencing the development of dental erosion *in vitro*: enamel type, temperature and exposure time. J Oral Rehabil 1999;26:624–630. [PubMed: 10447814]

Anderson P, Levinkind M, Elliott JC. Scanning microradiographic studies of rates of in vitro demineralization in human and bovine dental enamel. Arch Oral Biol 1998;43:649–656. [PubMed: 9758048]

Ando M, van Der Veen MH, Schemehorn BR, Stookey GK. Comparative study to quantify demineralized enamel in deciduous and permanent teeth using laser- and light-induced fluorescence techniques. Caries Res 2001;35:464–470. [PubMed: 11799288]

Angker L, Nockolds C, Swain MV, Kilpatrick N. Quantitative analysis of the mineral content of sound and carious primary dentine using BSE imaging. Arch Oral Biol 2004;49:99–107. [PubMed: 14693203]

Aoba T, Yagi T. Effects of acid-dissolution on thin ground sections of enamel caries studied by microradiography and x-ray microbeam diffraction. J Oral Pathol 1982;11:191–200. [PubMed: 6808098]

Arends J, Jongebloed WL. Mechanism of enamel dissolution and its prevention. J Biol Buccale 1977;5:219–237. [PubMed: 233844]

Arends J, Christoffersen J, Christoffersen MR, Øgaard B, Dijkman AG, Jongebloed WL. Rate and mechanism of enamel demineralization *in situ*. Caries Res 1992;26:18–21. [PubMed: 1568233]

Cuy JL, Mann AB, Livi KJ, Teaford MF, Weihs TP. Nanoindentation mapping of the mechanical properties of human molar tooth enamel. Arch Oral Biol 2002;47:281–291. [PubMed: 11922871]

Dowker SE, Elliott JC, Davis GR, Wassif HS. Longitudinal study of the three-dimensional development of subsurface enamel lesions during in vitro demineralisation. Caries Res 2003;37:237–245. [PubMed: 12771498]

Hunter ML, West NX, Hughes JA, Newcombe RG, Addy M. Erosion of deciduous and permanent dental hard tissue in the oral environment. J Dent 2000;28:257–263. [PubMed: 10722899]

Issa AI, Preston KP, Preston AJ, Toumba KJ, Duggal MS. A study investigating the formation of artificial sub-surface enamel caries-like lesions in deciduous and permanent teeth in the presence and absence of fluoride. Arch Oral Biol 2003;48:567–571. [PubMed: 12828985]

Johnson NW. Some aspects of the ultrastructure of early human enamel caries seen with the electron microscope. Arch Oral Biol 1967;12:1505–1521. [PubMed: 5237335]

Jongebloed WL, Molenaar I, Arends J. Morphology and size-distribution of sound and acid-treated enamel crystallites. Calcif Tissue Res 1975;19:109–123. [PubMed: 1203747]

Kerebel B, Daculsi G, Kerebel LM. Ultrastructural studies of enamel crystallites. J Dent Res 1979;58 (Spec Iss B):844–851. [PubMed: 283126]

LeGeros, RZ. Calcium phosphates in oral biology and medicine. Basel: Karger; 1991.

Linden LA, Bjõrkman S, Hattab F. The diffusion in vitro of fluoride and chlorhexidine in the enamel of human deciduous and permanent teeth. Arch Oral Biol 1986;31:33–37. [PubMed: 3085643]

Lippert F, Parker DM, Jandt KD. Susceptibility of deciduous and permanent enamel to dietary acid-induced erosion studied with atomic force microscopy nanoindentation. Eur J Oral Sci 2004;112:61–66. [PubMed: 14871195]

Lussi A, Kohler N, Zero D, Schaffner M, Megert B. A comparison of the erosive potential of different beverages in primary and permanent teeth using an *in vitro* model. Eur J Oral Sci 2000;108:110–114. [PubMed: 10768723]

Mafe S, Manzanares JA, Reiss H, Thomann JM, Gramain P. Model for the dissolution of calcium hydroxyapatite powder. J Phys Chem 1992;96:861–866.

Maupome G, Aguilar-Avila M, Medrano-Ugalde H, Borges-Yanez A. *In vitro* quantitative microhardness assessment of enamel with early salivary pellicles after exposure to an eroding cola drink. Caries Res 1999;33:140–147. [PubMed: 9892782]

Mullin, JW. Crystallization. Vol. 4. Oxford: Butterworth-Heinemann; 2001.

Naujoks R, Schade H, Zelinka F. Chemical composition of different areas of the enamel of deciduous and permanent teeth (the content of Ca, P, CO2, Na and N2). Caries Res 1967;1:137–143. [PubMed: 5232603]

Orams HJ, Phakey PP, Rachinger WA, Zybert JJ. Ultrastructural changes in the translucent and dark zones of early enamel caries. J Oral Pathol 1980;9:54–61. [PubMed: 6767822]

Pelton, AR.; Gronsky, R.; Williams, DB. Images of materials. Oxford: Oxford University Press; 1991.

Shellis RP. Relationship between human enamel structure and the formation of caries-like lesions in vitro. Arch Oral Biol 1984;29:975–981. [PubMed: 6598367]

Simmelink JW, Nygaard VK, Scott DB. Theory for the sequence of human and rat enamel dissolution by acid and by EDTA: a correlated scanning and transmission electron microscope study. Arch Oral Biol 1974;19:183–197. [PubMed: 4212466]

Sonju Clasen AB, Ogaard B, Duschner H, Ruben J, Arends J, Sonju T. Caries development in fluoridated and non-fluoridated deciduous and permanent enamel in situ examined by microradiography and confocal laser scanning microscopy. Adv Dent Res 1997;11:442–447. [PubMed: 9470502]

Tang R, Nancollas GH, Orme CA. Mechanism of dissolution of sparingly soluble electrolytes. J Am Chem Soc 2001;123:5437–5443. [PubMed: 11389624]

Tang R, Wang L, Orme CA, Bonstein T, Bush PJ, Nancollas GH. Dissolution at the nanoscale: self-preservation of biominerals. Angew Chem Int Ed 2004;43:2697–2701.

Tesch W, Eidelman N, Roschger P, Goldenberg F, Klaushofer K, Fratzl P. Graded microstructure and mechanical properties of human crown dentin. Calcif Tissue Int 2001;69:147–157. [PubMed: 11683529]

Tomson MB, Nancollas GH. Mineralization kinetics: a constant composition approach. Science 1978;200:1059–1060. [PubMed: 17740700]

Veis, A. Mineralization in organic matrix frameworks. In: Dove, PM.; De Yoreo, JJ.; Weiner, S., editors. Biomineralization. Reviews in mineralogy and geochemistry. Vol. 54. Washington, DC: The Mineralogical Society of America; 2003. p. 249-289.

Wang L, Tang R, Bonstein T, Orme CA, Bush PJ, Nancollas GH. A new model for nanoscale enamel dissolution. J Phys Chem B 2005;109:999–1005. [PubMed: 16866472]

Weiner, S.; Dove, PM. An overview of biomineralization processes and the problem of the vital effect. In: Dove, PM.; De Yoreo, JJ.; Weiner, S., editors. Biomineralization. Reviews in mineralogy and geochemistry. Vol. 54. Washington, DC: The Mineralogical Society of America; 2003. p. 1-29.

Wilson PR, Beynon AD. Mineralization differences between human deciduous and permanent enamel measured by quantitative microradiography. Arch Oral Biol 1989;34:85–88. [PubMed: 2783050]

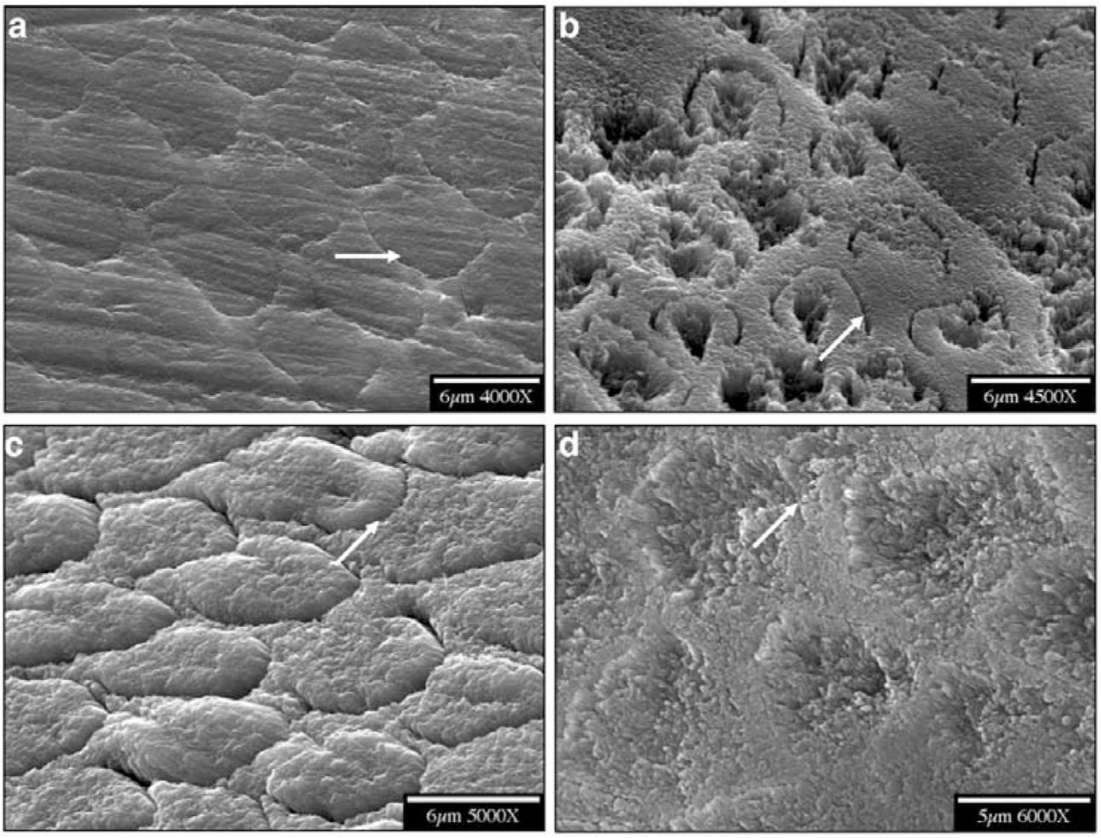

Figure 1.
SEMs of enamel before and after demineralization. **(a,b)** primary; **(c,d)** permanent. Arrows show that demineralization was initiated at the core/wall interfaces of rods and developed anisotropically along the c-axis.

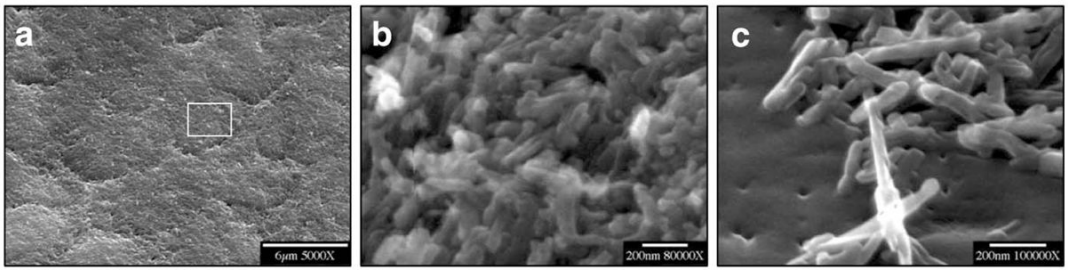

Figure 2.
SEM of nanosized crystallites. **(a)** Nanosized crystallites attached to primary enamel surface after initial dissolution. **(b)** Enlargement of the rectangular area in (a). **(c)** Nanosized crystallites collected from bulk solution by filtration during the initial linear stage of dissolution (as shown in Fig. 4e).

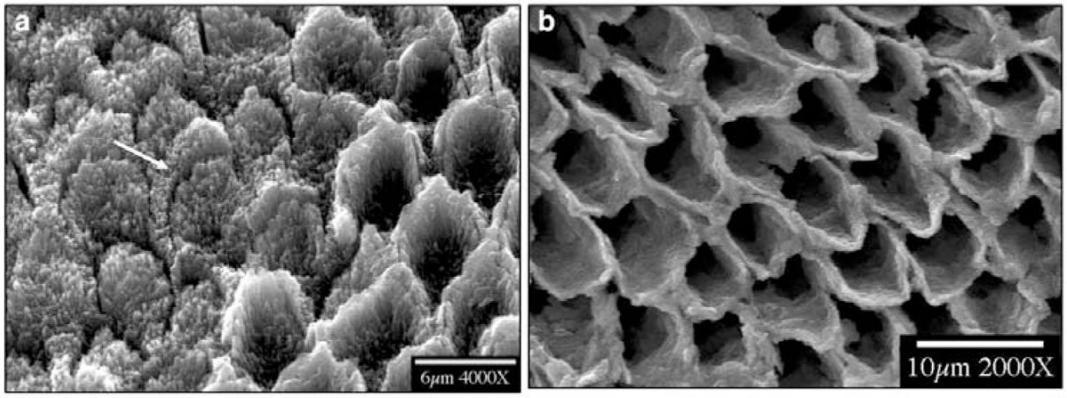

Figure 3.
SEMs of dissolving enamel cores, showing **(a)** the erosion of the walls of primary tooth enamel and **(b)** their retention for permanent tooth enamel after long-term dissolution. Arrow shows a fractured primary enamel wall.

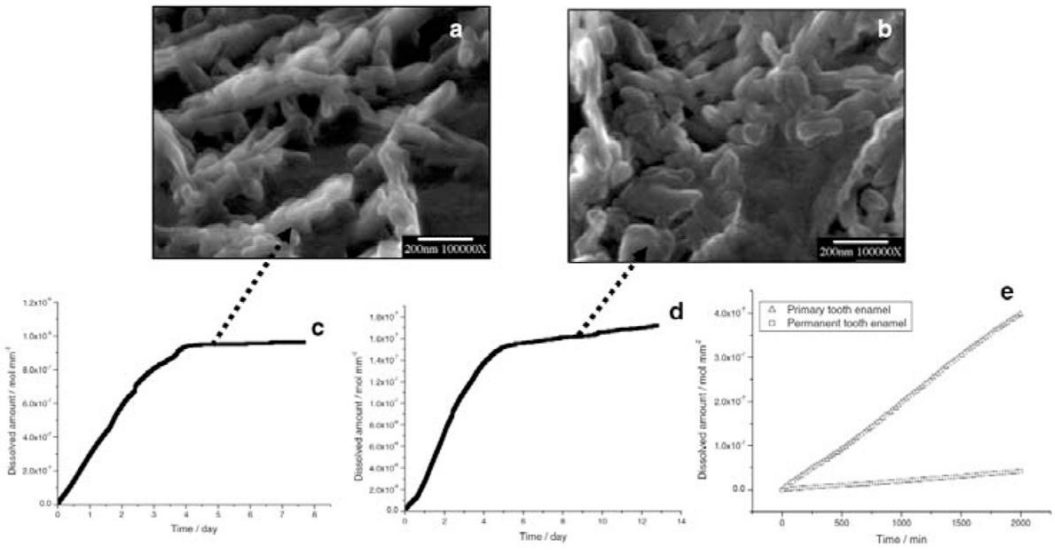

Figure 4.

Nanosized crystallites at the plateaux stages of dissolution of **(a)** primary and **(b)** permanent enamel collected by filtration from the bulk solution. CC curves of **(c)** primary and **(d)** permanent tooth enamel dissolution. The rates decreased virtually to zero at the end of dissolution reactions. **(e)** Comparison of dissolution rates of primary and permanent tooth enamel during the initial linear stages of dissolution.